LANGMUIR

pubs.acs.org/Langmuir Article

Experiments and Molecular Simulations to Study the Effect of Surface-Active Compounds in Mixtures of Model Oils on CO_2 Corrosion during Intermittent Oil–Water Wetting

Neda Norooziasl, Abolfazl Faeli Qadikolae, David Young, Bruce Brown, Sumit Sharma, and Marc Singer*

Cite This: https://doi.org/10.1021/acs.langmuir.4c00052 Read Online

ACCESS | Metrics & More | Article Recommendations | Supporting Information

ABSTRACT: Intermittent oil–water wetting can have a significant effect on the internal corrosion of steel pipelines. This paper presents a combined experimental and molecular modeling study of several influential factors on the surface properties and corrosion behavior of mild steel in CO_2 environments. The influence of different model oils (LVT-200 and Aromatic-200) and select surface-active compounds (myristic acid, cyclohexane butyric acid, and oleic acid) on the corrosion behavior of carbon steel during intermittent oil–water wetting was determined by measuring the corrosion rate after intermittent wetting cycles. The interfacial tension measurements were performed to study the incorporation of the oil phase along with surface-active molecules in the protective layer formed on the specimen surface. Results showed that the interfacial tension for an aromatic oil–water interface is lower than that for an aliphatic oil–water interface. To understand this result, molecular dynamics simulations of oil–water interfaces were performed in the presence of surface-active molecules and different oils to analyze the structure of the layer formed at the interface. The simulations supported the hypothesis that aromatic molecules are less structured at the interface, which results in the incorporation of more water molecules into the protective layer formed at the steel surface, causing a higher corrosion rate. On the other hand, the simulations revealed that myristic acid in an aliphatic oil forms a well-aligned structure at the interface, devoid of any water molecules. This is in agreement with the hypothesis that the linear molecular structure of myristic acid favors the alignment of molecules at an aliphatic oil–water interface, resulting in a lower interfacial tension and more effective corrosion mitigation as compared to the other two nonlinear compounds tested. It is concluded that an important factor controlling the corrosion behavior is the molecular structure of the oil–water interface, which is adopted by the steel surface layer through the Langmuir–Blodgett process.

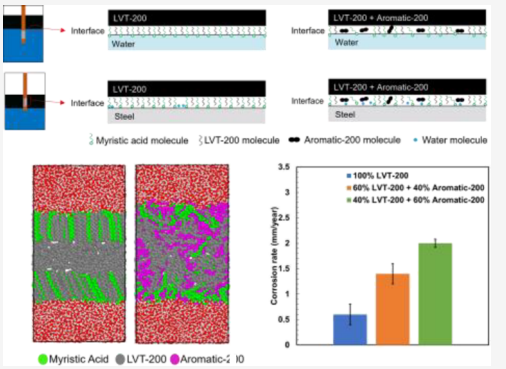

INTRODUCTION

Carbon steel pipelines are the most efficient and economical method for transporting oil and natural gas, especially for their large-scale transfer across long distances.[1,2] However, these pipelines are prone to corrosion due to the presence of corrosive gases such as carbon dioxide (CO_2) and/or hydrogen sulfide (H_2S) dissolved in the brine from the reservoir. CO_2 corrosion, also known as sweet corrosion, is one of the main problems in the oil and gas industry. CO_2 is very soluble in water and forms carbonic acid (H_2CO_3) upon hydration, which dissociates to bicarbonate (HCO_3^-), carbonate (CO_3^{2-}), and hydrogen ions (H^+). For the case of mild steel, the overall CO_2 corrosion reaction can be written as eq 1;

$$Fe + CO_2 + H_2O \rightarrow Fe^{2+} + CO_3^{2-} + H_2 \quad (1)$$

When iron from the steel undergoes oxidation in the presence of CO_2 and water (H_2O), resulting in the formation of ferrous ions (Fe^{2+}), hydrogen gas (H_2) is evolved because of reduction of hydrogen ions present in the water phase.[3] The oil phase itself does not lead to corrosion and can even prevent it.[4−7] In oil–water flow within a pipeline oriented horizontally at low flow rates, the water phase is present as a separate layer that flows in the lower section of the pipe. This represents a stratified flow pattern since the gravitational force becomes dominant over turbulent force. Increasing the flow rate in the pipeline augments the turbulent energy; consequently, the water phase may become gradually dispersed as droplets within the oil phase.[8−10] When considering pipelines operated at low water cut, the water phase is typically entrained by the

Received: January 4, 2024
Revised: March 23, 2024
Accepted: April 21, 2024

hydrocarbon phase, and the oil phase wets the internal surface of the pipe, removing any risk of corrosion. As the water content increases, water may break out and wet the internal surface of the pipeline more easily and potentially cause corrosion.[11−13] Considering the significant variability in production flow rates during the lifetime of a pipeline system, various flow regimes can occur in which oil and water phases can alternately wet the internal surface of the pipeline. This phenomenon is identified as "oil−water intermittent wetting".[14] Water content and flow velocity can influence the degree of oil−water intermittent wetting.[13] This phenomenon can affect the mechanism of the corrosion of the metal surface, which may be different from those generally accepted for aqueous CO_2 corrosion of mild steel (i.e., full water wetting).[4,8,15,16] The wetting condition of the metal surface is consequently a crucial factor to predict corrosion behavior,[17−20] and it is of great importance to determine the relation between wetting condition of the metal surface and corrosion processes.[21−23] This knowledge can help to decrease economic costs and mitigate the potential for adverse environmental impacts caused by corroding pipes.

Crude oils are naturally existing mixtures of hydrocarbons in liquid form (83−87 wt % of carbon, 10−14 wt % of hydrogen) that contains derivatives of nitrogen (0.1−2.0 wt %), oxygen (0.05−1.5 wt %), sulfur (0.05−6.0 wt %), metals (less than 1000 ppm), and other elements.[24−26] Some chemical compounds native to crude oils identified as surface-active compounds have an ability to preferentially adsorb at steel−water, steel−oil, and oil−water interfaces, which can alter the wetting and corrosion properties of steel surfaces.[8] Identifying all of the surface-active chemical compounds present in crude oils would be a challenging task. An alternative approach to testing whole crude oils is to select model compounds that are representative of the crude oil compounds. Although this approach utilizes a significantly simplified system compared to testing whole crude oils, it provides information about the contribution of specific groups of chemical compounds based upon their functionalities. Neumann et al. showed that surface-active compounds such as oxygen compounds, sulfur compounds, and nitrogen compounds affect the wettability preference of a crude oil.[27] Previously, the corrosion inhibition and wettability effect of oxygen containing compounds was studied[21,23]; in this paper, the effect of select carboxylic acid surface-active compounds on corrosion inhibition, interfacial tension, and oil−water interface structure is presented.

Studying the molecular orientation of surfactants at oil−water interfaces is challenging due to the limitations of experimental techniques at molecular scale resolutions. To address this problem, molecular dynamics simulations were performed to investigate the adsorption of surfactants at various oil−water interfaces to obtain molecular level insights. Molecular dynamics simulations have historically been employed to explore the interfacial behavior of surfactants. Previous studies successfully utilized molecular dynamics simulations to investigate micelle formation,[28−30] orientation of surfactant molecules at metal−water interfaces,[31,32] and specific cases of oil−water interfaces with and without surfactants.[33,34] Müller et al.,[33] conducted molecular dynamics simulations to study the adsorption behavior of linear ionic surfactants at octane−water interfaces. They demonstrated that as the concentration of the surfactants increased, interfacial tension decreased. Moreover, octane molecules have an impact on distribution of surfactant molecules at oil−water interfaces. Kunieda[34] observed the aggregation of aromatic molecules at oil−water interfaces. They concluded that weak hydrogen bonding between water molecules and aromatic rings is responsible for this behavior. However, no prior studies have been found performing molecular dynamics simulations to investigate the effect of oil type on orientation of nonionic linear surfactants at oil−water interfaces. Molecular dynamics simulations were performed using nonionic linear surfactants to study the orientation of surfactants at different oil−water interfaces and in different surfactant concentrations. The results revealed that in an aliphatic oil linear surfactant molecules align parallel to each other and to the oil molecules at the oil−water interface. In an aromatic oil, such a structural arrangement of linear surfactants is not observed. The simulation results play a pivotal role in understanding the intricacies of corrosion mechanisms in carbon steel pipelines subjected to oil−water two-phase flow. By elucidating the impact of intermittent oil−water wetting on corrosion processes, these findings offer crucial insights into the complex interplay between wetting conditions and corrosion behavior. Additionally, the molecular dynamics simulation provides valuable molecular-level perspectives on the adsorption behavior of surfactants at various oil−water interfaces. These simulations bridge the gap in understanding the orientation of nonionic linear surfactants under different oil types and concentrations, shedding light on the nuanced interfacial interactions that influence corrosion inhibition and interfacial tension. Ultimately, these simulation outcomes contribute to enhancing predictive models and strategies for mitigating corrosion risks, thereby reducing economic costs and environmental impacts associated with corroded pipelines.

EXPERIMENTAL AND SIMULATION SECTION

Materials and Chemicals. Two different model oils, paraffinic and aromatic, were used in the experiments. The paraffinic oil is LVT-200, which is a hydrotreated light distillate petroleum fraction.[35] The chemical composition of LVT-200 is shown in Table 1.

Table 1. Chemical Composition of LVT-200[35]

element	C_{12}	C_{13}	C_{14}	C_{15}	C_{16}	C_{17}
content, vol.%	1.8	20.1	39.7	33.1	4.6	0.7

The aromatic model oil is Aromatic-200, which contains a complex mixture of aromatic hydrocarbons that are predominantly derivatives of naphthalene.[36] The composition of the hazardous constituents of this oil is shown in Table 2.

Table 2. Chemical Composition of Aromatic-200[36]

constituents	1-methyl naphthalene	2-methyl naphthalene	naphthalene
concentration, wt %	<12.5%	<26.0%	<14.0%

The composition of crude oils is complicated and contains many different chemical compounds. Therefore, model oils containing selected dissolved species were used to simulate crude oil behaviors in order to isolate their influence. In this research, three different surface-active compounds were used in experiments with the same functional groups, carboxylic acids, and different aliphatic tails. These compounds are representative of naturally occurring surface-active compounds in crude oils. The chemical structures of these compounds are shown in Figure 1.

The metal specimens utilized for electrochemical measurements conducted in this study were machined from X65 carbon steel, which

https://doi.org/10.1021/acs.langmuir.4c00052
Langmuir XXXX, XXX, XXX−XXX

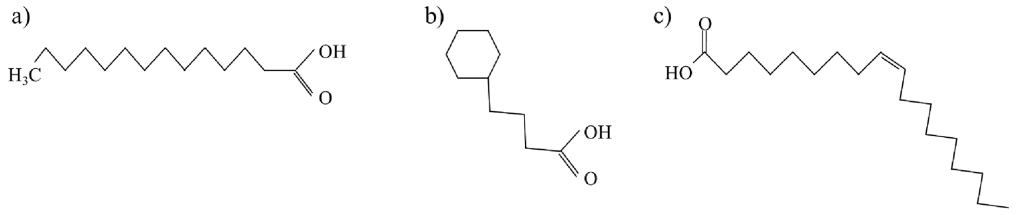

Figure 1. Chemical structure of (a) myristic acid ($C_{14}H_{28}O_2$), (b) cyclohexane butyric acid ($C_{10}H_{18}O_2$), and (c) oleic acid ($C_{18}H_{34}O_2$).

Table 3. Chemical Compositional Analysis of the X65 Pipeline Steel

element	C	Mn	Si	Ni	Cu	Cr	Mo	Al	Nb	P	S	Ti	V	Fe
wt %	0.05	1.40	0.22	0.24	0.11	0.23	0.07	0.023	0.036	0.003	<0.001	0.011	0.035	balance

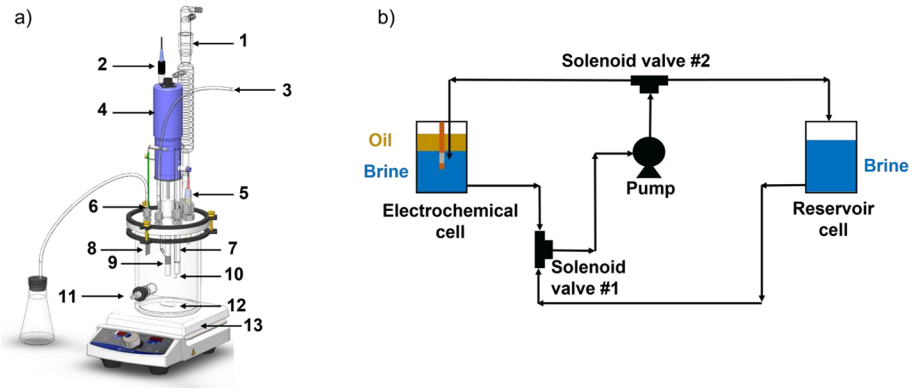

Figure 2. Schematic picture of (a) the glass cell: (1) condenser; (2) reference electrode; (3) brine inlet; (4) rotator; (5) pH probe; (6) gas outlet; (7) gas inlet; (8) counter electrode; (9) working electrode; (10) thermocouple; (11) brine outlet; (12) magnetic stir bar; (13) hot plate. (b) Intermittent wetting setup.

is a pipeline steel material used in the upstream oil and gas industry. This X65 carbon steel has a uniform, fine structure of cementite precipitates in a ferrite matrix and conforms to applicable specifications for API 5L, grade X65 seamless, or welded pipe with the following chemical analysis (Table 3).

Corrosion Rate Measurements. Experiments were performed in a standard three electrode glass cell with a carbon steel X65 rotating cylinder electrode (RCE) as the working electrode, a platinum-coated titanium mesh counter electrode, and a Ag/AgCl (KCl saturated) reference electrode. A schematic picture of the electrochemical glass cell is shown in Figure 2a. The electrochemical glass cell is connected to another reservoir glass cell to change the level of the water phase in the main glass cell, enabling alternate placement of the specimen in oil and water. These two glass cells are connected to each other by using a pump and two solenoid valves. A simple schematic of the intermittent wetting setup is shown in Figure 2.

Before each experiment, the RCE was sequentially polished with 400 and 600 grit silicon carbide abrasive papers, cleaned with 2-propanol in an ultrasonic bath, and air-dried. Both oil and water were deoxygenated for 1 h by sparging with CO_2 before the introduction of the working electrode. After the RCE was inserted into the glass cell, a precorrosion test was conducted to determine whether the initial corrosion rate was close to the blank test (to ensure repeatability) and to confirm no contamination from the previous test. The open circuit potential serves as a reference point for conducting linear polarization resistance assessments. The working electrode undergoes polarization within a range of ±5 mV around the open circuit potential. Linear polarization resistance (LPR) measurements were taken with a scan range from −5 to +5 mV vs open circuit potential (OCP), a scan rate of 0.125 mV/s, and a B value of 26 mV using a Gamry Interface 1010B potentiostat. To minimize the noise in electrochemical measurements caused by CO_2 sparging, the sparge tube was retracted into the headspace during data acquisition. The CO_2 corrosion rate is obtained by using Faraday's law:

$$\mathrm{CR} = \frac{i_{\mathrm{CORR}} M_{\mathrm{Fe}}}{\rho_{\mathrm{Fe}} 2F} \tag{2}$$

where CR is the corrosion rate in m/s (which could be converted to mm/year by a factor of 3.1536×10^{10}), M_{Fe} is the molecular mass of iron in kg/kmol, ρ_{Fe} is the density of iron in kg/m^3, F is the Faraday constant, F = 96.485 C/kmol, and i_{CORR} is the corrosion current density, A/m^2, which is obtained by eq 3 (Stern−Geary equation)[37,38];

$$i_{\mathrm{CORR}} = \frac{B}{R_{\mathrm{p}} A} \tag{3}$$

The B value used here is taken from previous research conducted on mild steel in a CO_2 environment,[39] which equals to 0.026 V; R_{p} is the polarization resistance corrected by solution resistance (R_{s}) in ohms ($R_{\mathrm{p}} = R_{\mathrm{p}'} - R_{\mathrm{s}}$); $R_{\mathrm{p}'}$ is the polarization resistance measured by LPR; R_{s} is the resistance of the electrolyte solution measured by the electrochemical impedance spectroscopy (EIS) technique; and A is the working electrode surface area in m^2. The solution was purged with CO_2 throughout the test to prevent air ingress and to saturate the test solution with CO_2. The pH was adjusted by adding a deoxygenated hydrochloric acid or sodium bicarbonate solution during each experiment. The test matrix used to study the presence of oil on corrosion rate is outlined in Table 4.

These experiments were performed in four steps:

1. Precorrosion: polished specimen was immersed in the water phase. This step allows for formation of corrosion products, i.e., iron carbide (Fe_3C) under the operating conditions of this study, thereby mimicking real-world conditions observed within the internal surfaces of oil and gas pipelines.
2. Partitioning: 300 mL of an oil layer containing surface-active compounds was added to the top of the water phase. The

https://doi.org/10.1021/acs.langmuir.4c00052
Langmuir XXXX, XXX, XXX−XXX

Table 4. Test Matrix to Study the Effect of Intermittent Wetting on the Corrosion Rate

parameter	conditions
material	X65
water phase	1 wt. % NaCl in DI water
oil phase	100% LVT-200,60% LVT-200 and 40% Aromatic-200,40% LVT-200 and 60% Aromatic-200 (15% of total liquid)
temperature	30 °C
CO_2 partial pressure	0.96 bar
pH	4.0
RCE rotational speed	1000 rpm
intermittent wetting period	1 min.
duration of intermittent wetting	1 h
surface-active compound	myristic acid, 4-cyclohexyl butyric acid, oleic acid (0.1 wt. % of oil phase)
experimental equipment	RCE, Glass cell
electrochemical measurements	OCP, LPR, EIS (electrochemical impedance spectroscopy)

polished specimen was still immersed into the water phase and rotated for 1 h at 1000 rpm.

3. Intermittent wetting: The intermittent wetting step includes two substeps:
   a. Oil wetting step: brine is pumped from the electrochemical cell to the reservoir cell to lower the oil layer, so the oil layer completely surrounds the specimen surface.
   b. Water wetting step: brine is pumped from the reservoir cell back to the electrochemical cell to lift the oil layer well above the specimen surface.[40]
4. Persistency: After intermittent wetting cycles, the specimen was returned to the water phase. The corrosion rate was measured every 20 min for at least 10 h.

Interfacial Tension Measurements. Interfacial tension is the measure of free energy per unit area of interface between two liquid phases and it could help to characterize changes that occur at the oil–water interfaces.[41,42] Oil–water interfacial tension measurements were performed to evaluate the surface activities of acidic compounds. The measurements were done using the K20 KRÜSS tensiometer and Wilhelmy plate method described in the Supporting Information, SI. Both 1 wt. % NaCl solution and LVT-200 containing surface-active compounds were sparged with CO_2 for at least 1 h. The temperature and pH of both were adjusted to the same values as for electrochemical measurements before each measurement. Measurements were performed with 30–50 mL of each phase. Each measurement was repeated at least three times.

Molecular Dynamics Simulations. Molecular dynamics simulations were performed using Groningen Machine for Chemical Simulations (GROMACS) simulation package.[43] Water molecules were modeled using the extended single point charge (SPCE) model, and tetradecane, 1-methyl naphthalene, and myristic acid molecules were modeled using the optimized potentials for liquid simulations (OPLS)-AA force field employed.[44,45] LigParGen Web site was used to generate the three-dimensional structure and molecular topology parameters of the organic molecules.[46−48] PACKMOL software was employed to create initial configurations.[49]

The simulation box size was nominally $L_x \times L_X \times L_z$ = 5 nm × 5 nm × 10 nm. The central region of the simulation box was filled with oil molecules, either tetradecane or 60% tetradecane and 40% 1-methylnaphthalene, so that the oil phase occupied roughly half the height of the simulation box in the z dimension. The regions above and below the oil phase were filled with water molecules. The surfactant molecules were placed close to the interfaces in the oil phase in random orientations and locations to reduce the diffusion time needed for them to reach the interface. Figure S3 displays a visualization of the initial simulation box.[50−52]

The Leap-Frog algorithm with a time step of one fs was used for integrating the equation of motion. van der Waals interactions were represented by the Lennard-Jones functional form. Particle mesh Ewald (PME) summation was employed for long-range Coulombic interactions in all three dimensions. A spherical cutoff of 1.4 nm was chosen for Lennard–Jones and real-space component of Ewald summation was employed for Coulombic interactions. Periodic boundary conditions (PBC) were applied in all three dimensions and hydrogen atoms were constrained using the LINCS algorithm.[53]

Simulations proceeded as follows: initially, an energy minimization with the steepest-descent algorithm was performed. Subsequently, a 100 ps equilibration was carried out in the canonical ensemble (NVT). This was followed by $NL_xL_yP_zT$-ensemble simulation, where the system pressure was controlled by adjusting the L_z dimension of

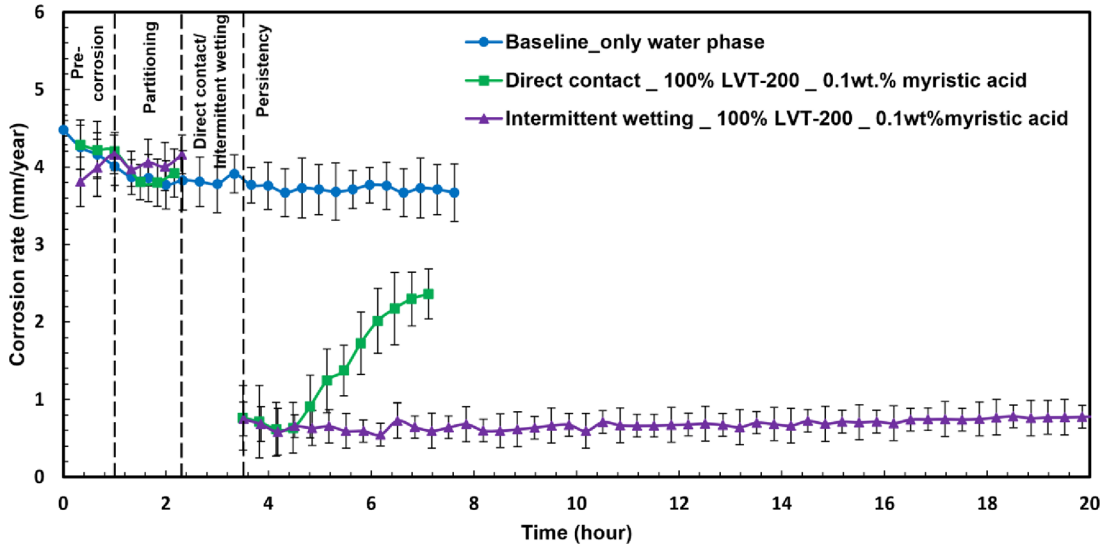

Figure 3. Corrosion rate in the presence of LVT-200 containing 0.1 wt. % myristic acid at pH 4.0, 30 °C, 0.96 bar CO_2, and 1000 rpm for 1 h direct contact with oil and 1 h intermittent wetting.

https://doi.org/10.1021/acs.langmuir.4c00052
Langmuir XXXX, XXX, XXX−XXX

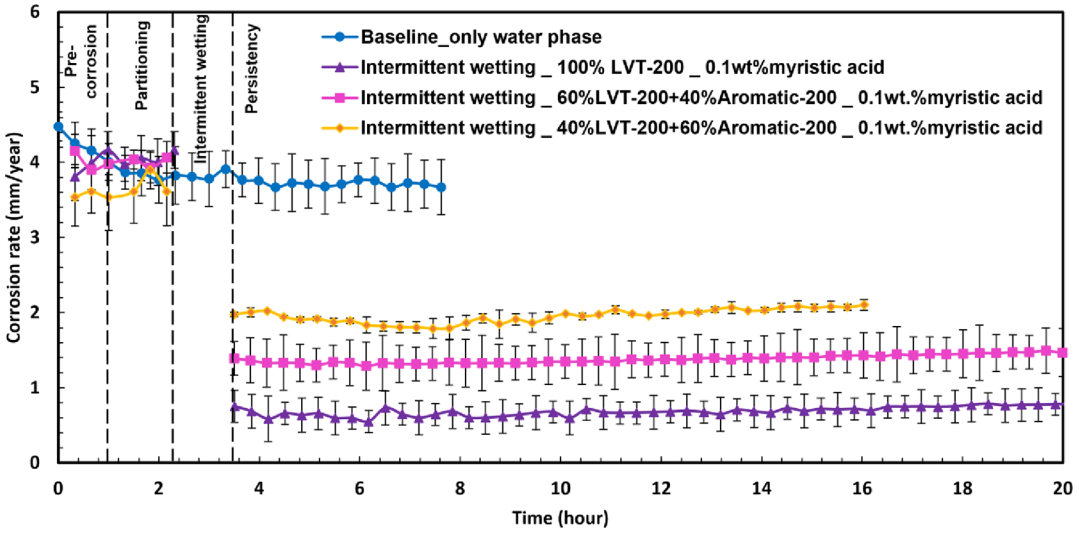

Figure 4. Corrosion rate in the presence of mixtures of LVT-200 and Aromatic-200 containing 0.1 wt. % myristic acid at pH 4.0, 30 °C, 0.96 bar CO_2, and 1000 rpm under 1 h intermittent wetting condition.

the box using Berendsen barostat (τp = 2 ps) and temperature was controlled by v-rescale temperature coupling (τT = 0.2 ps). After 100 ns, the pressure coupling was switched to Parrinello−Rahman with the same time constant. Equilibrium was achieved after 250 ns for all of the simulations, which was determined by ensuring that the molecular configurations at the interface are no longer evolving with time. Finally, a 50 ns production run was conducted to analyze the configurations.

The interfacial tension is calculated using the Kirkwood method based on the anisotropy in pressure tensors. The formula used is $\gamma = -L_z\left[\frac{P_x + P_y}{2} - P_z\right]/N_{\text{int}}$[54] where L_z is the simulation box size in the Z direction, P_x is pressure component at x direction, and N_{int} corresponds to the number of interfaces in the simulation box, determined from density profile in the Z axis. Pressure components and density profiles were obtained by using GROMACS internal tools.

RESULTS AND DISCUSSION

Corrosion Rate Results. *Effect of Different Model Oils.* The results for corrosion rate experiments at pH 4.0, 30 °C, 0.96 bar of CO_2, and 1000 rpm are shown in Figure 3. They include a "baseline-water phase only" experiment, which is compared with tests involving "direct contact" and "intermittent wetting" conditions, using LVT-200 containing 0.1 wt. % myristic acid. The "baseline-water phase only" experiment shows the corrosion rate of mild steel in the presence of only a water phase, i.e., no oil phase is present in the experimental glass cell. This test was stopped after ∼7.5 h of stable corrosion rate. In the "direct contact" experiment, the specimen was continuously immersed in the oil phase for one hour after the precorrosion and partitioning steps. The corrosion rate did not change in the partitioning step, but there was a significant decrease in the corrosion rate after the direct contact with the hydrocarbon phase that was persistent for approximately one hour before the corrosion rate began to gradually increase. In the "intermittent wetting" experiment, the specimen was periodically immersed in each phase for 1 min and this cycle was repeated for 1 h. For "intermittent wetting", it was observed that the corrosion rate did not change in the partitioning step; however, the significant decrease measured after the intermittent wetting cycles remained persistent for more than 17 h. A possible explanation for this difference is related to the number of times the specimen surface was moved through the oil−water interface. Myristic acid has a sufficiently high hydrophobicity and low solubility in water, so that a higher concentration of myristic acid would be observed at the oil−water interface where it could promote the development of a more persistent layer as the specimen surface was moved multiple times through the oil−water interface, as compared to one-time direct contact.[40] Given that the specimen under examination is an X65 carbon steel with a mere 0.05 wt % carbon content, a limited quantity of corrosion products, particularly iron carbide (Fe_3C), is anticipated to develop. This means that the progress of the experiments over a few hours (precorrosion and partitioning steps) does not affect the roughness of the surface and consequently the adsorption of the surfactants significantly. Babic showed that the roughness of X65 specimen corroding at 25 °C and pH 5 changes from 0.16 μm before corrosion to 0.19 μm after 2 h of precorrosion, and the same roughness value was obtained even after 8 h of precorrosion. Their SEM images showed that a very limited amount of carbide was formed after 2 h of precorrosion in a way that the polishing mark were still noticeable on the specimen surface.[23] Moreover, as mentioned earlier, the precorrosion step simulates the roughness of internal surface of pipelines on the X65 carbon steel surface.

In order to investigate the effect of an aromatic oil on the corrosion behavior of mild steel, the oil composition was changed from 100% LVT-200 to two different mixtures of LVT-200 and Aromatic-200. The results for corrosion rate experiments under intermittent wetting condition in the presence of mixtures of LVT-200 and Aromatic-200 containing 0.1 wt. % myristic acid are shown in Figure 4. In these experiments, the same intermittent wetting procedure was used. It was observed that, by addition of 40% Aromatic-200 to the oil phase mixture, the corrosion rate increased from ∼0.6 to ∼1.4 mm/y, and by further increasing the Aromatic-200 oil phase mixture ratio to 60%, the corrosion rate increased more to ∼2 mm/y. It seems that the presence of aromatic oil decreases the corrosion mitigation effect of the film formed on the specimen surface, which results in a higher corrosion rate.

This phenomenon can be explained by the Langmuir and Langmuir−Blodgett concepts. Amphiphilic substances insolu-

https://doi.org/10.1021/acs.langmuir.4c00052
Langmuir XXXX, XXX, XXX−XXX

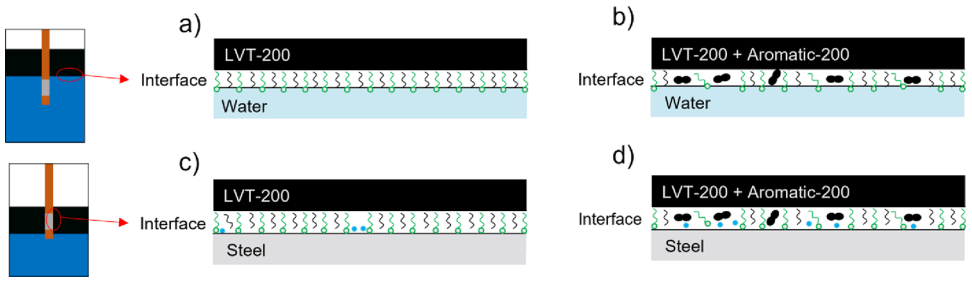

Figure 5. Schematics of the structures of film formed at (a) LVT-200/water, (b) LVT-200 and Aromatic-200/water, (c) LVT-200/steel, and (d) LVT-200 and Aromatic-200/steel interfaces (Myristic acid molecule, LVT-200 molecule, Aromatic-200 molecule, and water molecule).

ble in water can be easily spread on an air−water (oil−water) interface to form a monolayer. These monolayers are called Langmuir (L) films. The monolayer is adsorbed to a solid substrate when the substrate is dipped up and down through the monolayer formed at the air−water (oil−water) interface. These mono/multilayer structures are called Langmuir−Blodgett (LB) films.[55]

A possible mechanism is proposed in terms of the structure of the film formed at the oil−water and steel-oil interfaces to explain the effect of aromatic oil on the corrosion behavior of steel, which is explained with the help of the schematics shown in Figure 5. As shown in these schematics, it is hypothesized that the linear LVT-200 molecules and the hydrophobic tail of myristic acid molecules align at the LVT-200/water interface due to hydrophobic interactions (Figure 5a). This results in the formation of a well-oriented and highly packed film at the interface. However, the presence of aromatic molecules breaks the alignment of oil and surfactant molecules at the interface (Figure 5b), which results in a less organized layer. Fewer LVT-200 molecules are available at the interface to attract the myristic acid molecules in the presence of Aromatic-200 oil. Moreover, a weak hydrogen bond between aromatic molecules and water molecules favors the presence of aromatic molecules at the oil−water interface rather than being distributed in the bulk of oil phase.[34,56]

When the specimen is brought in contact with the oil−water interface, the layer formed at the interface is transferred to the specimen surface (Figure 5c,d). Furthermore, the flow disturbance could entrain water molecules into the interface film at the steel surface. In the presence of Aromatic-200 oil, more water molecules can be incorporated into the surface film because of the weak hydrogen bonds between aromatic and water molecules (Figure 5d).

Furthermore, the interfacial tension between oil−water interfaces were measured. The water/LVT-200 interfacial tension was measured to be 48 ± 1.4 mN/m, while the water/(60%LVT-200 + 40%Aromatic-200) interfacial tension was 37.6 ± 0.8 mN/m. The lower interfacial tension measured in the presence of Aromatic-200 can be attributed to the weak hydrogen bond between aromatic and water molecules. The effect of Aromatic-200 on interfacial tension can also be seen visually in Figure 6. All the vials contain 50% NaCl solution and 50% oil, with the composition of the oil phase shown in Table 5 for each sample. The vials were shaken, and the photo was taken 1 min later. It was observed that an oil phase with a higher ratio of Aromatic-200 leads to more stable entrainment of water molecules into the oil phase which agrees with interfacial tension results, i.e., lower interfacial tension between water/Aromatic-200 causes more incorporation of the water molecules into the surface film.

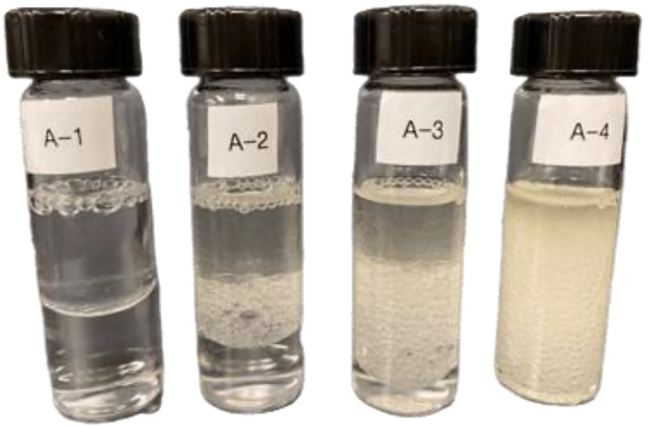

Figure 6. Images showing the entrainment of water molecules when different volume percentage of Aromatic-200 is added to the oil phase (composition of each shown in Table 5).

Table 5. Composition of the Oil Phase in Sample Vials

sample	vol. % of LVT-200 in the oil phase	vol. % of Aromatic-200 in the oil phase
A-1	100	0
A-2	60	40
A-3	40	60
A-4	0	100

The measured interfacial tension values and the corresponding corrosion rates are shown in Figure 7. The measured interfacial tension at water/LVT-200 interface was 48 ± 1.4 mN/m, which decreased to 36.2 ± 2.3 mN/m by the addition of 0.1 wt % myristic acid to the oil phase. The corresponding corrosion rate decreased from 4.0 to 0.6 mm/y. The same trend was observed for the water/(60%LVT-200 + 40% Aromatic-200) system. The measured interfacial tension at water/(60%LVT-200 + 40%Aromatic-200) interface was 37.6 ± 0.8 N/m, which decreased to 25.4 ± 1.6 mN/m by the addition of 0.1 wt % myristic acid to the oil phase. The corresponding corrosion rate also decreased from 4.0 to 1.4 mm/y. Therefore, in these experiments, a decrease in the interfacial tension is typically associated with a decrease in the corrosion rate. However, this may not be generally true. The absolute value of interfacial tension is system dependent and may not always result in a decrease in the corrosion rate.

Effect of Different Surface-Active Compounds. In order to investigate the effect of the chemical structure of surface-active compounds on the corrosion behavior of mild steel, two other surface-active compounds, 4-cyclohexyl butyric acid and oleic acid, were dissolved in the oil phase. The results of corrosion

https://doi.org/10.1021/acs.langmuir.4c00052
Langmuir XXXX, XXX, XXX−XXX

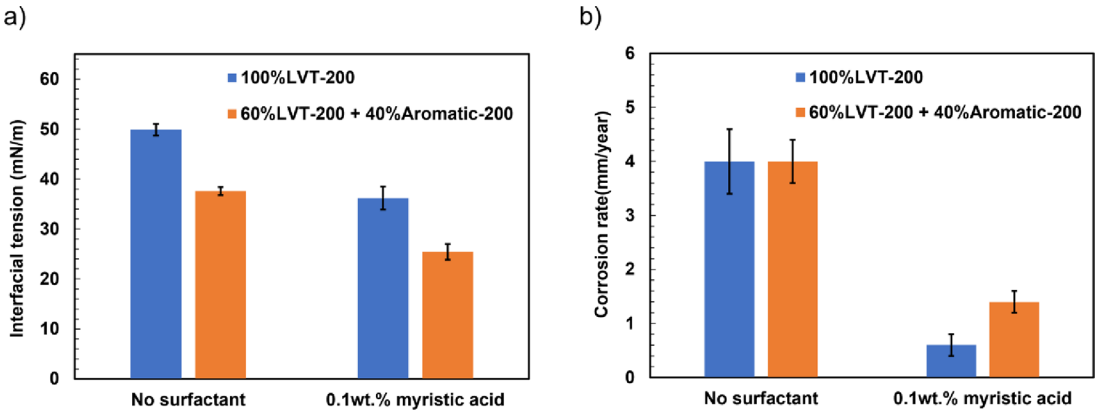

Figure 7. (a) Oil–water interfacial tensions (IFT) and (b) correlated corrosion rates in the presence of myristic acid at pH 4.0 and 30 °C.

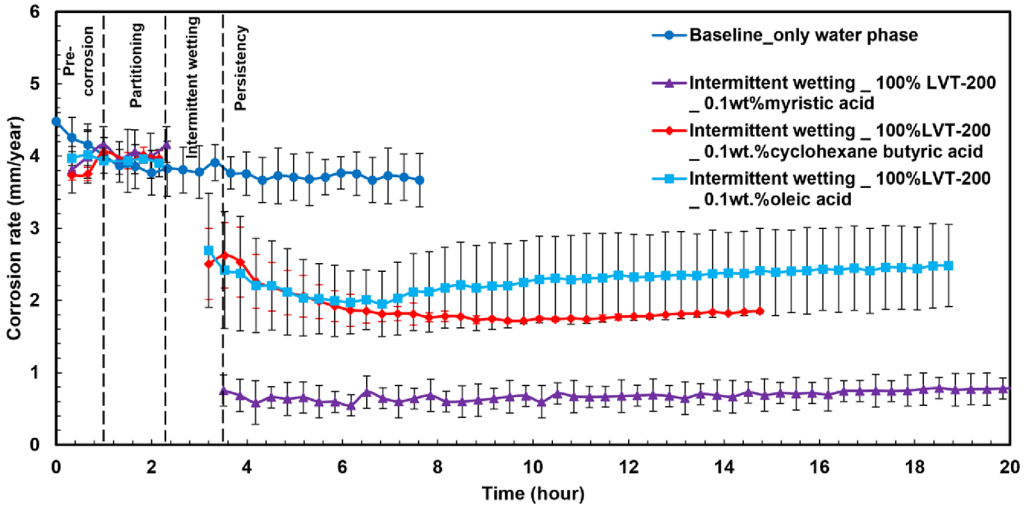

Figure 8. Corrosion rate in the presence of LVT-200 containing 0.1 wt % myristic acid, 4-cyclohexyl butyric acid, or oleic acid at pH 4.0, 30 °C, 0.96 bar CO_2, and 1000 rpm under 1 h intermittent wetting conditions.

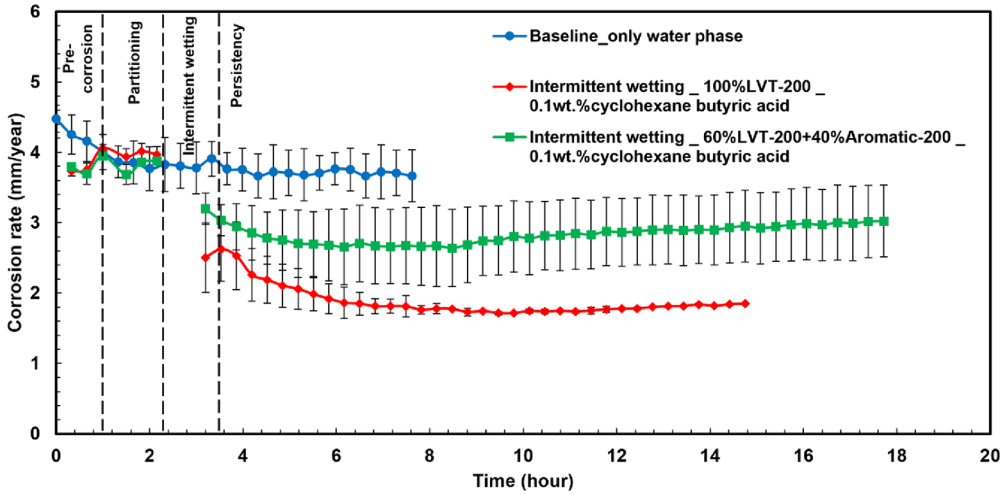

Figure 9. Corrosion rate in the presence of LVT-200 and mixture of 60% LVT-200 and 40% Aromatic-200 containing 0.1 wt % 4-cyclohexyl butyric acid at pH 4.0, 30 °C, 0.96 bar CO_2, and 1000 rpm under 1 h intermittent wetting condition.

rate experiments under intermittent wetting condition in the presence of LVT-200 containing 0.1 wt % myristic acid, 4-cyclohexyl butyric acid, and oleic acid are shown in Figure 8. In this experiment, the specimen was periodically immersed in each phase for one min and this cycle was repeated for one h (intermittent wetting procedure). It was observed that by the addition of 4-cyclohexyl butyric acid or oleic acid to the oil phase, the corrosion rate increased from ~0.6 to ~1.8 and ~2.2 mm/y, respectively. Therefore, the presence of nonlinear surface-active compounds, 4-cyclohexyl butyric acid and oleic

https://doi.org/10.1021/acs.langmuir.4c00052
Langmuir XXXX, XXX, XXX−XXX

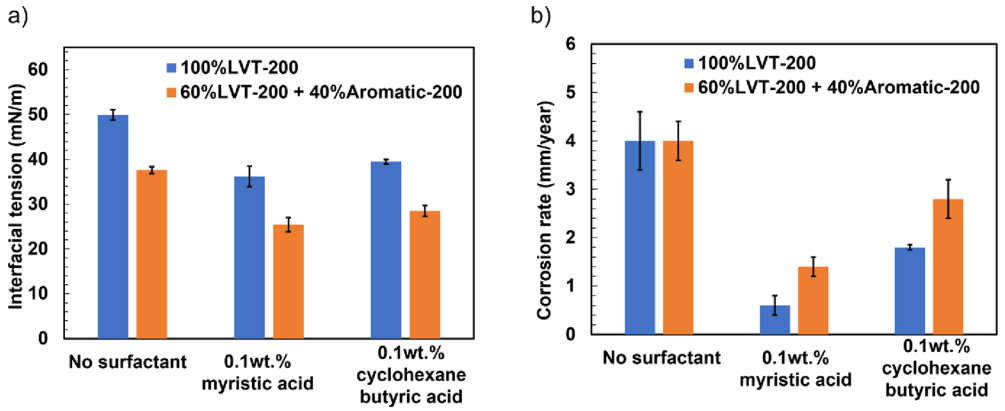

Figure 10. (a) Oil–water interfacial tensions and (b) correlated corrosion rates in the presence of myristic acid and 4-cyclohexane butyric acid at pH 4.0 and 30 °C.

acid, decreases the corrosion mitigation effect of the film formed on the specimen surface and results in a higher corrosion rate. This is hypothesized to be the result of poor alignment of LVT-200 molecules and nonlinear surface-active compounds at the oil–water interface, which results in formation of a loosely packed and consequently less corrosion protective interface layer. The smaller hydrophobic interactions between nonlinear surfactants and oil molecules in comparison to linear surfactant (myristic acid) and oil molecules may account for this behavior.

The effect of the presence of aromatic oil on the corrosion mitigation behavior of 4-cyclohexyl butyric acid was also studied. The results of the corrosion rate experiments under intermittent wetting conditions in the presence of LVT-200 and a mixture of LVT-200 and Aromatic-200 containing 0.1 wt % 4-cyclohexyl butyric acid are shown in Figure 9. It was observed that by addition of 40% Aromatic-200 to the oil phase mixture, the corrosion rate increased from ∼1.8 to ∼2.8 mm/y. This observation is in agreement with our hypothesis that the presence of aromatic oil decreases the corrosion mitigation effect of the film formed on the specimen surface and results in a higher corrosion rate.

Interfacial tension was also measured in the presence of 4-cyclohexyl butyric acid. The measured interfacial tension values at the oil/water interface and the corresponding corrosion rates are shown in Figure 10. The interfacial tension at water/LVT-200 interface in the presence of myristic acid and 4-cyclohexyl butyric acid was measured as 36.2 ± 2.3 and 39.5 ± 0.5 mN/m, respectively. The same trend was observed for water/(60% LVT-200 + 40% Aromatic-200) interface. The interfacial tension values are slightly higher in the presence of 4-cyclohexyl butyric acid at both interfaces as compared to the results in the presence of myristic acid, which agrees with the corrosion rate results.

Molecular Dynamics Simulation Results. Two distinct model oils were employed to investigate the adsorption of surface-active compounds (surfactants) at oil–water interfaces. The first simulation system consisted of tetradecane, chosen to represent LVT-200, which is a linear oil. The second system was composed of a mixture containing 60% tetradecane and 40% 1-methylnaphthalene. 1-Methylnaphthalene represents Aromatic-200, which is an aromatic model oil. Myristic acid was used as a surfactant in the simulations and, number of surfactant molecules, $N \in \{0,15,30,45\}$ were placed in the oil phase close to each interface in the simulation box. The number of surfactants used in the simulations is determined by the concentration values employed in the experiments. The concentration of surfactant at the interface may be calculated from surface or interfacial tension data by use of the appropriate Gibbs eq (eq 4).[57]

$$d\gamma = -\sum_i \Gamma_i d\mu_i \tag{4}$$

For solutions of a nonionic surfactant:

$$\Gamma_1 = -\frac{1}{2.303RT}\left(\frac{\partial\gamma}{\partial \log C_1}\right) \tag{5}$$

where γ [mN/m] is the interfacial tension, R = 8.31 J/mol.K, C_1 is the mole fraction, and Γ_1 [mol/1000m^2] is the concentration of surfactants per area. The calculated number of surfactants based on the bulk concentration is shown in Table 6.

Table 6. Number of Molecules at 25 nm^2 Interface Calculated from Their Bulk Concentration

bulk concentration (wt % in oil)	IFT (mN/m)	Γ (mol/1000m^2)	Γ (#molecules/nm^2)	number of molecules at 25 nm^2
0.1	38	0.002126989	1.28	32.02
1.0	34	0.00281764	1.69	42.41

LVT-200/Water Interface. Adsorption behavior of different concentrations of myristic acid at the LVT-200/water interface was studied. Snapshots of the equilibrium morphologies are shown in Figure 11a–c. Myristic acid surfactants absorbed at the interfaces, and no exchange of surfactants between the interfaces was observed during the simulations. As it is shown in Figure 11a, at low concentrations of myristic acid, myristic acid and LVT-200 (tetradecane) do not attain any ordered arrangement at the interface. As the concentration is increased (Figure 11b,c), strong hydrophobic interactions between the tail of myristic acid and LVT-200 molecules led to their alignment parallel to each other, resulting in the formation of a well-oriented film at the interface.

To quantify the molecular orientation of LVT-200 molecules at the interface in the presence of different numbers of myristic acid surfactants, the angle between the surface normal and the end-to-end vector of LVT-200 molecules was calculated (Figure 12a). Figure 12a shows that while there is a uniform

https://doi.org/10.1021/acs.langmuir.4c00052
Langmuir XXXX, XXX, XXX−XXX

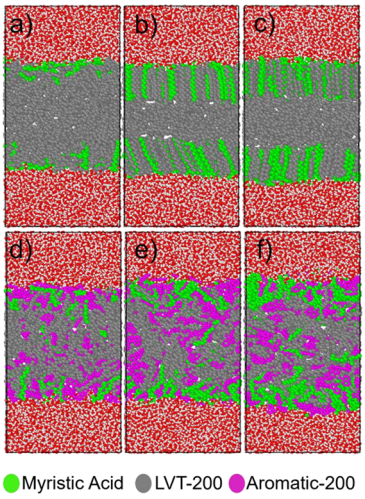

Figure 11. Snapshots of equilibrium morphologies for (a) 15, (b) 30, and (c) 45 myristic acid surfactants at each initial LVT-200 (represented by tetradecane)/water interface. The snapshots (d–f) show the system with 15, 30, and 45 surfactants, respectively, with LVT-200 (tetradecane) and Aromatic-200 (represented by1MN)/water interface.

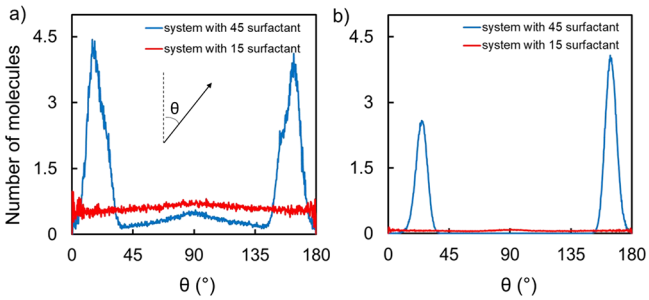

Figure 12. Distribution of the angle between interfacial surface normal and end to end vector of (a) LVT-200 and (b) myristic acid molecules for two different concentrations. At small concentration, the LVT-200 and myristic acid molecules do not have any preferred orientation. At the higher concentration, the distributions show sharp peaks close to 0 and 180° because of the alignment of both these molecules perpendicular to the interface.

distribution of angles at low concentration of surfactants, at higher concentration, the distribution of orientation of LVT-200 molecules is sharply peaked at angles close to 0 and 180°, which is attributed to the formation of a well-oriented structure wherein the LVT-200 molecules are aligned perpendicular to the interface. Figure 12b shows the distribution of the orientations of myristic acid for the two concentrations. Myristic acid aligns parallel to LVT-200 molecules at the higher concentration but does not attain any preferred orientation at the low concentration.

Mixture of LVT-200 and Aromatic-200/Water interface. Adsorption behavior of different concentrations of myristic acid at the LVT-200 and Aromatic-200/water interfaces was studied next. Snapshots of the equilibrium morphologies are illustrated in Figure 11d–f. As shown in Figure 13, in the presence of Aromatic-200 molecules, no favored alignment of the surfactants and the oil molecules was observed regardless of the surfactant concentration, in contrast with simulations without Aromatic-200 (Figure 12). Hydrophobic interactions between LVT-200 and myristic acid molecules are weakened in the presence of Aromatic-200. The density profiles of the

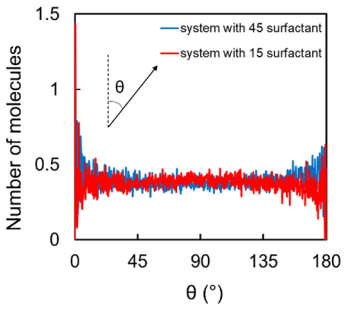

Figure 13. Distribution of the angle between interfacial surface normal and end to end vector of LVT-200 in the presence of Aromatic-200 molecules for two different surfactants concentrations.

system with 30 myristic acid molecules along the *Z*-axis are shown in Figure 14. It is observed that Aromatic-200

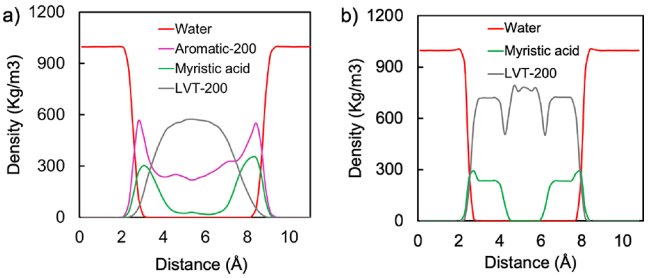

Figure 14. Density profiles of compounds for (a) mixture of LVT-200 and Aromatic-200 system with 30 myristic acid molecules at each interface and (b) LVT-200 system with 30 myristic acid molecules at each interface.

molecules tend to adsorb more on to the oil–water interface as compared to LVT-200. The presence of Aromatic-200 at the interface disrupts the alignment of LVT-200 and myristic acid. These simulation results confirm our hypothesis that linear oil molecules align with linear myristic acid molecules to form a well-packed hydrophobic film at the oil–water interface, which gets transferred to the solid substrate during intermittent wetting experiment. The presence of nonlinear oil molecules disrupts the formation of this film and so only weak inhibition is observed.

Comparison of Two Interface Systems Based on Experimental and Simulation Results. Electrochemical measurements showed that corrosion mitigation due to the oil phase decreases with the addition of aromatic oil (1-methylnaphthalene) to the oil mixture (Figure 15). It is proposed that the presence of aromatic molecules disrupts the alignment of linear oil and surfactant molecules at the interface (Figure 5c,d). Fewer LVT-200 molecules are at the interface to interact with the myristic acid molecules in the presence of Aromatic-200 oil. Moreover, a weak hydrogen bond between aromatic molecules and water molecules favors the aggregation of aromatic molecules at the interface. This also leads to entrainment of water molecules into the interface layer in the presence of aromatic oil. Molecular dynamics simulations showed that Aromatic-200 is aggregated at the oil–water interface and disrupts the organization of LVT-200 and myristic acid molecules at the interface. The interfacial tension values obtained from both experiments and simulations are compared in Figure 16. The Kirkwood method was used to calculate the interfacial tension from molecular simulations.

https://doi.org/10.1021/acs.langmuir.4c00052
Langmuir XXXX, XXX, XXX–XXX

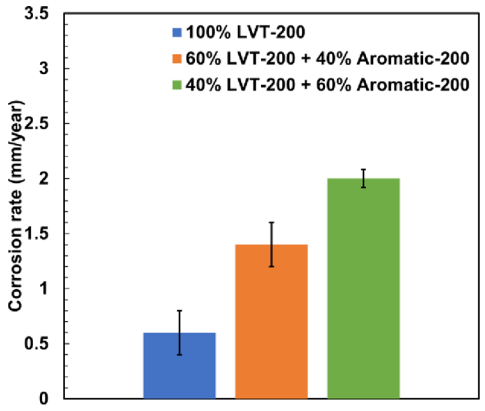

Figure 15. Corrosion rate in the presence of different model oils containing 0.1 wt % myristic acid at pH 4.0, 30 °C, 0.96 bar CO_2, and 1000 rpm after 1 h intermittent wetting condition.

The number of interfaces differs when there is a parallel orientation of myristic acid and LVT-200 molecules. Figure S4 shows the density profiles and the number of interfaces for LVT-200/water systems in the *Z* direction for the systems with different concentrations of myristic acid. Local stresses in the simulation system were calculated using GROMACS-LS.[58−61] As shown in Figure S5, there is a change in the number of interfaces at the microscopic level when surfactants and oil molecules are aligned parallel to each other. Even though surfactant concentrations in the experiments cannot be directly mapped to the number of surfactants in molecular simulations, the experiments and simulations showed similar trends, as shown in Figure 16. As discussed in the previous section, the lower interfacial tension measured in the presence of the aromatic oil can be attributed to the weak hydrogen bond between aromatic and water molecules.

It is imperative to acknowledge that the impact of oil/surfactants on the CO_2 corrosion rate is a combination of oil/water and steel/liquid interfacial processes. However, under the conditions of this study, it can be assumed that the steel surface adopts the structure of the oil/water interface layer during intermittent wetting stage since (i) the corrosion rate results align with IFT results and (ii) the surface morphology of the X65 specimen does not change significantly during precorrosion and partitioning steps.

The effect of surface-active compounds on the CO_2 corrosion behavior of X65 carbon steel is a broad research area and has been a continuous research endeavor. Previous studies have shown that surfactant compounds interact with the oil molecules at the steel interface and consequently provide corrosion mitigation. The CO_2 corrosion mitigation effect is dependent on the chemical structure of the molecules, as well as the physical properties of the aqueous phase and operational conditions.[62] It has also been shown that surfactants mostly block the active sites of the surface and reduce the corrosion rate,[63] and in a few cases, the adsorbed layer on the surface is thick enough to provide a mass transfer barrier. Although, caution needs to be taken in interpreting the results of these works since they focus on the adsorption of inhibitor surfactants without the presence of the hydrocarbon phase.

CONCLUSIONS

- The linear structure of myristic acid favors the alignment of linear oil molecules perpendicular to the aliphatic oil−water interface resulting in the formation of a film that strongly inhibits corrosion and reduces interfacial tension.
- Molecular dynamics simulations showed that LVT-200 and myristic acid align perpendicular to the interface at high concentrations of surfactants, which is consistent with low corrosion rate observed in these systems.
- Nonlinear surface-active compounds (4-cyclohexyl butyric acid and oleic acid) are unable to align perpendicular to the oil−water interface and manifest higher interfacial tension and lower corrosion mitigation, as a result.
- In the presence of Aromatic-200 oil, the interfacial alignment of oil molecules and surfactants is disrupted. A high corrosion rate is observed in these systems.
- The interfacial tension for an aromatic oil−water interface is lower than that of an aliphatic oil−water interface because of the weak hydrogen bonding between aromatic molecules and water molecules.

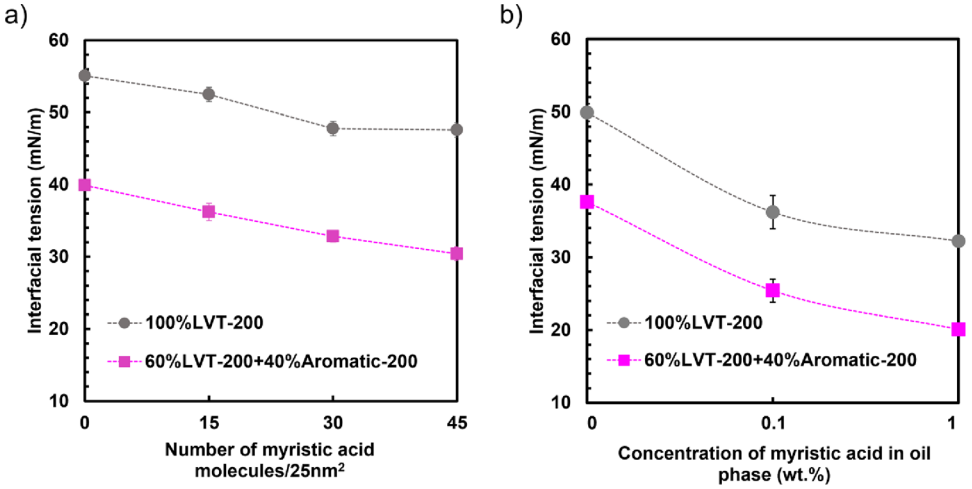

Figure 16. Oil−water interfacial tension values for different myristic acid concentrations obtained from (a) simulations of mixture of tetradecane and Aromatic-200 at 30 °C and (b) experiments for mixture of LVT-200 and Aromatic-200 at pH 4.0 and 30 °C.

https://doi.org/10.1021/acs.langmuir.4c00052
Langmuir XXXX, XXX, XXX−XXX

Therefore, aromatic oil incorporates more water molecules into the protective layer formed at the steel surface, which leads to a higher corrosion rate.

■ ASSOCIATED CONTENT

Supporting Information

The Supporting Information is available free of charge at https://pubs.acs.org/doi/10.1021/acs.langmuir.4c00052.

Methodology and principle of oil/water interfacial tension measurement; snapshot of simulation box; density profiles of LVT-200/water interface; profile of pressure component in the z direction (P_z) (PDF)

■ AUTHOR INFORMATION

Corresponding Author

Marc Singer − *Department of Chemical and Biomolecular Engineering, Ohio University, Athens, Ohio 45701, United States;* orcid.org/0000-0002-0762-9755; Email: singer@ohio.edu

Authors

Neda Norooziasl − *Department of Chemical and Biomolecular Engineering, Ohio University, Athens, Ohio 45701, United States;* orcid.org/0000-0002-5196-2643

Abolfazl Faeli Qadikolae − *Department of Chemical and Biomolecular Engineering, Ohio University, Athens, Ohio 45701, United States;* orcid.org/0000-0002-6555-8895

David Young − *Department of Chemical and Biomolecular Engineering, Ohio University, Athens, Ohio 45701, United States;* orcid.org/0000-0002-1077-9586

Bruce Brown − *Department of Chemical and Biomolecular Engineering, Ohio University, Athens, Ohio 45701, United States*

Sumit Sharma − *Department of Chemical and Biomolecular Engineering, Ohio University, Athens, Ohio 45701, United States;* orcid.org/0000-0003-3138-5487

Complete contact information is available at: https://pubs.acs.org/10.1021/acs.langmuir.4c00052

Notes

The authors declare no competing financial interest.

■ ACKNOWLEDGMENTS

The authors would like to thank the following companies for their financial support: Ansys, Baker Hughes, Chevron Energy Technology, Clariant Corporation, ConocoPhillips, ExxonMobil, M-I SWACO (Schlumberger), Multi-Chem (Halliburton), Occidental Oil Company, Pertamina, Saudi Aramco, Shell Global Solutions, and TotalEnergies. S.S. would like to acknowledge the National Science Foundation (NSF) CAREER grant 2046095. Computational resources for this project were provided by NSF ACCESS grant DMR190005.

■ REFERENCES

(1) Revie, R. W. *Oil and gas pipelines: integrity and safety handbook*. John Wiley & Sons. 2015.

(2) Mansoori, H.; Esmaeilzadeh, F.; Mowla, D.; Mohammadi, A. H. Case study: production benefits from increasing C-values. *Oil Gas J.* **2013**, *111* (6), 64−73.

(3) Nesic, S.; Kahyarian, A.; Choi, Y. S. Implementation of a comprehensive mechanistic prediction model of mild steel corrosion in multiphase oil and gas pipelines. *Corrosion Journal.* **2019**, *75*, 274−291.

(4) Efird, K. D.; Jasinski, R. J. Effect of the crude-oil on corrosion of steel in crude oil brine production. *Corrosion.* **1989**, *45* (2), 165−171.

(5) Hernandez, S.; Bruzual, J.; Linares, F. L.; Luzon, J. G. Isolation of potential corrosion inhibiting compounds in crude oil. In *NACE Corrosion*, International Corrosion Conference Series. 2003, 03330.

(6) Hernandez, S.; Duplat, S.; Vera, J. R.; Baron, E.. A statistical approach for analyzing the inhibiting effect of different types of crude oil in CO2 corrosion of carbon steel. In *NACE Corrosion*, International Corrosion Conference Series. 2002, 02293.

(7) Hernandez, S.; Vera, J. R.; Mendez, C.; Duplat, S. On the mechanism of corrosion inhibition by crude oils. In *NACE Corrosion*, International Corrosion Conference Series. 2001, 01044.

(8) Brauner, N.; Ullmann, A. Modeling of phase inversion phenomenon in two-phase pipe flows. *Int. J. Multiphase Flow* **2002**, *28* (7), 1177−1204.

(9) Cai, J.; Li, C.; Tang, X.; Ayello, F.; Richter, S.; Nesic, S. Experimental study of water wetting in oil−water two phase flow—horizontal flow of model oil. *Chem. Eng. Sci.* **2012**, *73*, 334−344.

(10) Kee, K. E. A study of flow patterns and surface wetting in gas-oil-water flow. Ph.D. Dissertation. Ohio University, 2014.

(11) Ayello, F.; Li, C.; Tang, X.; Cai, J.; Nesic, S.; Cruz, C. I. T.; Al-Khamis, J. N. Determination of phase wetting in oil-water pipe flows. In *NACE Corrosion*, International Corrosion Conference Series, 2008, 08566.

(12) Kee, K. E.; Richter, S.; Babic, M.; Nesic, S. Flow patterns and water wetting in oil-water two phase flow−a flow loop study. In *NACE Corrosion*, International Corrosion Conference Series, 2014, 4068.

(13) Kee, K. E.; Richter, S.; Babic, M.; Nešić, S. Experimental Study of Oil-Water Flow Patterns in a Large Diameter Flow Loop - The Effects on Water Wetting and Corrosion. *Corrosion* **2016**, *72* (4), 569−582.

(14) Kermani, M. B.; Harrop, D. The impact of corrosion on the oil and gas industry. *SPE Prod. Facil.* **1996**, *11* (3), 186−190.

(15) Craig, B. D. Corrosion in oil/water systems. *Mater. Perform.* **1996**, *35* (8), 61−62.

(16) Smart, J. S. Wettability- A major factor in oil and gas system corrosion. *Mater. Perform.* **2001**, *40* (4), 54−59.

(17) Foss, M.; Gulbrandsen, E.; Sjoblom, J. Alteration of wettability of corroding carbon steel surface by carbon dioxide corrosion inhibitors— Effect on carbon dioxide corrosion rate and contact angle. *Corrosion.* **2008**, *64*, 905−919.

(18) Li, C.; Richter, S.; Nešić, S. How do inhibitors mitigate corrosion in oil-water two-phase flow beyond lowering the corrosion rate? *Corrosion* **2014**, *70*, 958−966.

(19) Thomas, R. R.; Brusic, V. A.; Rush, B. M. Correlation of surface wettability and corrosion rate for benzotriazole-treated copper. *J. Electrochem. Soc.* **1992**, *139* (3), 678−685.

(20) Wang, P.; Zhang, D.; Qiu, R.; Wan, Y.; Wu, J. Green approach to fabrication of a super-hydrophobic film on copper and the consequent corrosion resistance. *Corros. Sci.* **2014**, *80*, 366−373.

(21) Ayello, F. Crude Oil Chemistry Effects on Corrosion Inhibition and Phase Wetting in Oil-Water Flow. Ph.D. Dissertation, Ohio University, 2010.

(22) Zheng, L.; Wang, Z. M.; Song, G. Electrochemical characterization of an oil-water alternately wetted rotating cylinder electrode. *Corrosion* **2021**, *77* (1), 72−84.

(23) Babic, M. Role of interfacial chemistry on wettability and carbon dioxide corrosion of mild steels. Ph.D. Dissertation. Ohio University, 2017.

(24) Anderson, W. G. Wettability literature survey- part 1: rock/oil-brine interactions and the effects of core handling on wettability. *J. Pet. Technol.* **1986**, *38* (10), 1125−1144.

(25) Speight, J. G. *The chemistry and technology of petroleum*. Fifth ed., CRC Press, 2014.

(26) Schobert, H. *Chemistry of fossil fuels and biofuels*. Cambridge University Press, 2013.

(27) Neumann, H. J.; Paczynska-Lahme, B.; Severin, D. *Geology of petroleum*. Halsted Press: New York, 1985, 125.
(28) Marrink, S. J.; Tieleman, D. P.; Mark, A. E. Molecular Dynamics Simulation of the Kinetics of Spontaneous Micelle Formation. *J. Phys. Chem. B* **2000**, *104* (51), 12165−12173.
(29) Yoshii, N.; Iwahashi, K.; Okazaki, S. A molecular dynamics study of free energy of micelle formation for sodium dodecyl sulfate in water and its size distribution. *J. Chem. Phys.* **2006**, *124*, No. 184901.
(30) Fujiwara, S.; Itoh, T.; Hashimoto, M.; Horiuchi, R. Molecular dynamics simulation of amphiphilic molecules in solution: Micelle formation and dynamic coexistence. *J. Chem. Phys.* **2009**, *130*, No. 144901.
(31) Faeli Qadikolae, A.; Sharma, S. Facet Selectivity of Cetyltrimethyl Ammonium Bromide Surfactants on Gold Nanoparticles Studied Using Molecular Simulations. *J. Phys. Chem. B* **2022**, *126* (48), 10249−10255.
(32) Faeli Qadikolae, A.; Sharma, S. Molecular simulations of adsorption of surfactant micelles on partially and fully covered iron surfaces. *J. Mol. Liq.* **2023**, *379*, No. 121685.
(33) Müller, P.; Bonthuis, D. J.; Miller, R.; Schneck, E. Ionic Surfactants at Air/Water and Oil-Water Interfaces: A Comparison Based on Molecular Dynamics Simulations. *J. Phys. Chem. B* **2021**, *125* (1), 406−415.
(34) Kunieda, M.; et al. Self-Accumulation of Aromatics at the Oil−Water Interface through Weak Hydrogen Bonding. *J. Am. Chem. Soc.* **2010**, *132* (51), 18281−18286.
(35) Deep South Chemicals, *LVT 200 Material Safety Data Sheet*. 2014, Microsoft Word - LVT 200 (deep-south-chemical.com).
(36) Exxon Mobil, *Aromatic 200 Fluid Product Safety Summary*. 2020, https://ehslegacy.unr.edu/msdsfiles/34819.pdf.
(37) Stern, M. A method for determining corrosion rates from linear polarization data. *Corrosion* **1958**, *14* (9), 60−64.
(38) Stern, M.; Geary, A. L. Electrochemical polarization, 1. A theoretical analysis of the shape of polarization curves. *J. Electrochem. Soc.* **1957**, *104* (12), 751−752.
(39) Belarbi, Z.; Farelas, F.; Singer, M.; Nešić, S. Role of amine in the mitigation of CO_2 TOP of the line corrosion. *Corrosion* **2016**, *72* (10), 1300−1310.
(40) Norooziasl, N.; Young, D.; Brown, B.; Singer, M. Effect of Oil/Water Intermittent Wetting on CO2 Corrosion in the Presence of Acridine and Myristic Acid. *CORROSION* **2024**, *80*, 102−112.
(41) Rudin, J.; Wasan, D. T. Mechanisms for lowering of interfacial tension in alkali/acidic oil systems 1. Experimental studies. *Colloids Surf.* **1992**, *68*, 67−79.
(42) Rudin, J.; Wasan, D. T. Mechanisms for lowering the interfacial tension in alkali/acidic oil systems − 2. *Theoretical studies. Colloids and surfaces.* **1992**, *68*, 81−94.
(43) Abraham', M. J.; et al. GROMACS: High performance molecular simulations through multi-level parallelism from laptops to supercomputers. *SoftwareX* **2015**, *1-2*, 19−25.
(44) Berendsen, H. J. C.; Grigera, J. R.; Straatsma, T. P. The missing term in effective pair potentials. *J. Phys. Chem.* **1987**, *91* (24), 6269−6271.
(45) Jorgensen, W. L.; Maxwell, D. S.; Tirado-Rives, J. Development and Testing of the OPLS All-Atom Force Field on Conformational Energetics and Properties of Organic Liquids. *J. Am. Chem. Soc.* **1996**, *118* (45), 11225−11236.
(46) Jorgensen, W. L.; Tirado-Rives, J. Potential energy functions for atomic-level simulations of water and organic and biomolecular systems. *Proc. Natl. Acad. Sci. U. S. A.* **2005**, *102*, 6665−6670.
(47) Dodda, L. S.; Cabeza de Vaca, I.; Tirado-Rives, J.; Jorgensen, W. L. LigParGen web server: an automatic OPLS-AA parameter generator for organic ligands. *Nucleic Acids Res.* **2017**, *45*, W331−W336.
(48) Dodda, L. S.; Vilseck, J. Z.; Tirado-Rives, J.; Jorgensen, W. L. 1.14*CM1A-LBCC: Localized Bond-Charge Corrected CM1A Charges for Condensed-Phase Simulations. *J. Phys. Chem. B* **2017**, *121*, 3864−3870.
(49) Martínez, L.; Andrade, R.; Birgin, E. G.; Martínez, J. M. PACKMOL: A package for building initial configurations for molecular dynamics simulations. *J. Comput. Chem.* **2009**, *30*, 2157−2164.
(50) Darden, T.; York, D.; Pedersen, L. Particle mesh Ewald: An N·log(N) method for Ewald sums in large systems. *J. Chem. Phys.* **1993**, *98*, 10089−10092.
(51) Essmann, U.; Perera, L.; Berkowitz, M. L.; Darden, T.; Lee, H.; Pedersen, L. G. A smooth particle mesh Ewald method. *J. Chem. Phys.* **1995**, *103*, 8577−8593.
(52) Allen, M. P.; Tildesley, D. J. *Computer Simulation of Liquids*. Oxford University Press, 2017.
(53) Hess, B.; Bekker, H.; Berendsen, H. J. C.; Fraaije, J. G. E. M. LINCS: A linear constraint solver for molecular simulations. *J. Comput. Chem.* **1997**, *18*, 1463−1472.
(54) Kirkwood, J. G.; Buff, F. P. The Statistical Mechanical Theory of Surface Tension. *J. Chem. Phys.* **1949**, *17*, 338−343.
(55) https://www.nanoscience.com/techniques/langmuir-films/.
(56) Gierszal, K. P.; et al. π-Hydrogen Bonding in Liquid Water. *J. Phys. Chem. Lett.* **2011**, *2* (22), 2930−2933.
(57) Rosen, M. J. *Surface and Interfacial Phenomena*. Wiley, 2004.
(58) Vanegas, J. M.; Torres-Sanchez, A.; Arroyo, M. Importance of Force Decomposition for Local Stress Calculations in Biomembrane Molecular Simulations. *J. Chem. Theory Comput.* **2014**, *10*, 691−702.
(59) Vanegas, J. M.; Arroyo, M. Force Transduction and Lipid Binding in MscL: A Continuum-molecular Approach. *PLoS One* **2014**, *9*, No. e113947.
(60) Torres-Sanchez, A.; Vanegas, J. M.; Arroyo, M. Examining the Mechanical Equilibrium of Microscopic Stresses in Molecular Simulations. *Phys. Rev. Lett.* **2015**, *114*, No. 258102.
(61) Torres-Sanchez, A.; Vanegas, J. M.; Arroyo, M. Geometric Derivation of Microscopic Stress: A Covariant Central Force Decomposition. *J. Mech. Phys. Solids.* **2016**, *93*, 224−239.
(62) He, Y.; Wang, X.; Young, D.; Mohamed-Said, M.; Ren, S.; Singer, M. Electrochemical Study of Corrosion Inhibition of Carbon Steel During Oil/Water Intermittent Wetting. *J. Electrochem. Soc.* **2023**, *170*, No. 111502.
(63) Belarbi, Z.; Dominguez Olivo, J. M.; Farelas, F.; Singer, M.; Young, D.; Nesic, S. Decanethiol as a corrosion inhibitor for carbon steels exposed to aqueous CO_2. *Corrosion Journal.* **2019**, *75*, 1246−1254.

https://doi.org/10.1021/acs.langmuir.4c00052
Langmuir XXXX, XXX, XXX−XXX